ACS APPLIED MATERIALS & INTERFACES

Research Article

www.acsami.org

Label-Free Electrochemiluminescent Immunosensor for Detection of Carcinoembryonic Antigen Based on Nanocomposites of GO/MWCNTs-COOH/Au@CeO_2

Xuehui Pang, Jianxiu Li, Yongbei Zhao, Dan Wu, Yong Zhang, Bin Du, Hongmin Ma,* and Qin Wei*

Key Laboratory of Chemical Sensing & Analysis in Universities of Shandong, School of Chemistry and Chemical Engineering, University of Jinan, Jinan 250022, P.R. China

ABSTRACT: A high-sensitivity electrochemiluminescence (ECL) sensor was conducted to detect carcinoembryonic antigen (CEA). Nanocomposites of graphene oxide/carboxylated multiwall carbon nanotubes/gold/cerium oxide nanoparticles (GO/MWCNTs-COOH/Au@CeO_2) were used as antibody carriers and sensing platforms to modify on glassy carbon electrodes (GCE). CeO_2 nanoparticles were first exploited as an ECL luminescent material and the possible ECL mechanism was proposed in this work. GO/MWCNTs-COOH was used as a loading matrix for CeO_2 nanoparticles because of the superior conductivity and large specific surface area. Au nanoparticles were further deposited on this matrix to attach anti-CEA and enhance the sensitivity of immunosensor. The proposed sensing platform showed excellent cathodic ECL performance and sensitive response to CEA. The effects of experimental conditions on the ECL performance were investigated. The proposed immunosensor showed the broad linear range (0.05−100 ng/mL) and the low detection limit (LOD, 0.02 ng/mL, signal-to-noise ratio = 3) according to the selected experimental conditions. The excellent analysis performance for determination of CEA in the human serum samples simplied this immunosensor displayed high sensitivity and excellent repeatability. More importantly, this conducted immunosensor broadens the use scope of CeO_2 nanoparticles.

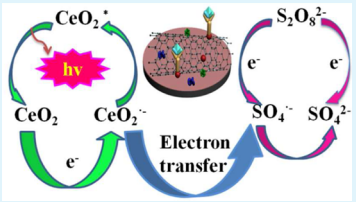

KEYWORDS: *carbon nanomaterials, modified electrodes, electrochemiluminescence, label-free immunosensor, cancer biomarker*

INTRODUCTION

In recent years, electrochemiluminescence (ECL) biosensors have been developed to detect biological analytes because of the weak background signal, high sensitivity, and simplified optical setup.[1−4] Apart from the traditional ECL system (tris-bipyridyl ruthenium[5] and luminol[6]), various nanomaterials, such as CdS,[7,8] CdSe,[9,10] CdTe,[11] CuS,[12] and CdS/ZnO,[13] have been exploited as ECL luminophors to fabricate biosensors with high sensitivity and selectivity. However, As far as we know, the investigation about ECL application of nanostructured metal oxides is less well reported. Herein, CeO_2 nanoparticles were used as luminescent materials for the first time.

Nanostructured metal oxides have exhibited big surface area and good reaction activity and are potential candidates for the fabrication of biosensors.[14] Nanostructured CeO_2 has aroused wide interest in the development of implantable biosensors because of biocompatibility and high chemical stability.[15,16] However, CeO_2 suffers from the low electron conductivity, which seriously affect their electrocatalytic efficiency.[17] To overcome this shortcoming, Qiu[18] and Saha[19] have prepared CeO_2@MWCNTs and nanoporous CeO_2 thin films to improve the conductivity and surface-to-volume ratio to detect hydrogen peroxide and glucose, respectively. Composites of GO and MWCNTs-COOH with superior electron conductivity and large specific surface area were adopted as large matrix for loading luminescent or catalytic material.[20,21] Because of $\pi-\pi$ restacking of GO, the electrochemical properties of the GO were limited. Therefore, a measure need to be taken to avoid the GO sheets restacking[22] and MWCNTs could be the candidate material[20,21,23,24] due to their remarkable thermal, mechanical, and electrical properties derived from their unique structure,[25−28] high aspect ratio and long-range $\pi-\pi$ conjugation. Therefore, the advantages of MWCNTs/GO and CeO_2 were combined to fabricate ECL sensing system for the first time, which showed great sensing performance.

Cancer is a great challenge and the detection of cancer biomarkers is significant for early diagnosis of cancer and clinical research.[29−32] CEA is a clinical tumor marker for early diagnosis of ovarian carcinoma, breast tumors and cervical carcinomas.[33,34] The increase of CEA level in serum above the normal value is an indication of possible disease.[35] Therefore, novel materials or methods would be explored for the detection of clinical tumor marker. For example, nanoparticles are used in biosensing.[36−38]

Herein, a highly sensitive label-free ECL immunosensor was fabricated to detect CEA. GO/MWCNTs-COOH/Au@CeO_2 served as the sensing platform for the first time. A one-step in situ method was used to disperse Au and CeO_2 nanoparticles on the surface of GO/MWCNTs-COOH. CeO_2 was utilized first for the luminescence. Anti-CEA was combined with the Au nanoparticles via the Au-NH_2 covalent bond to further enhance the sensitivity of immunosensor. This fabricated sensor had a wide linear range (0.05−100 ng/mL) and LOD (0.02 ng/mL).

Received: June 11, 2015
Accepted: August 14, 2015
Published: August 14, 2015

DOI: 10.1021/acsami.5b05185
ACS Appl. Mater. Interfaces 2015, 7, 19260−19267

Scheme 1. Schematic Diagram for Fabrication of the Label-Free ECL Immunosensor

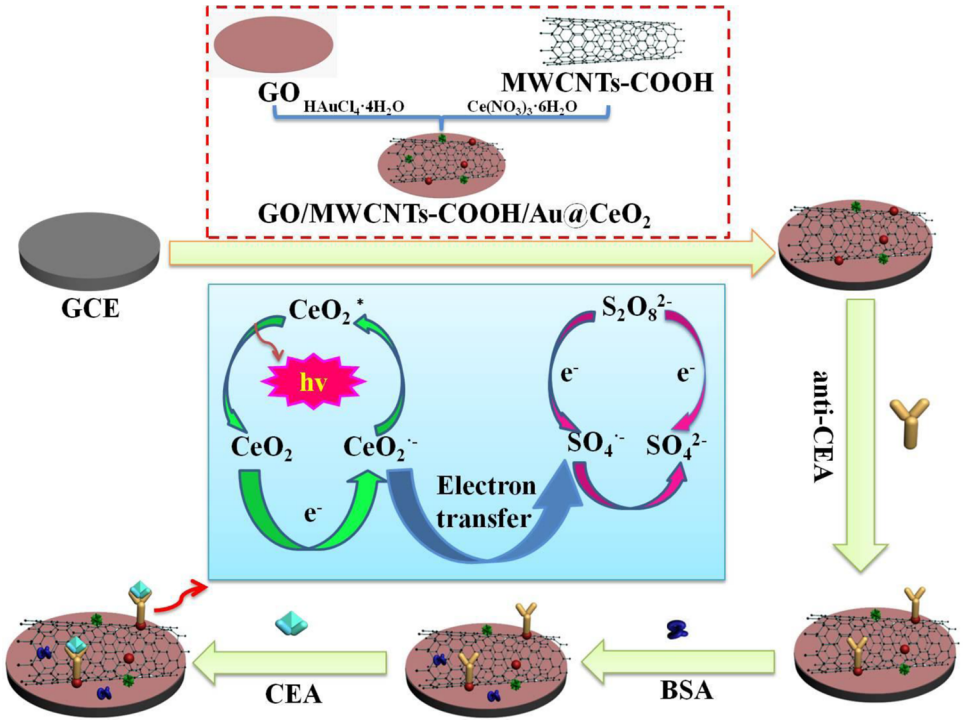

EXPERIMENTAL SECTION

Materials. Cerium nitrate hexahydrate ($Ce(NO_3)_3·6H_2O$) was purchased from Aladdin Co., Ltd. (Shanghai, China). MWCNTs-COOH was purchased from Chengdu Organic Chemicals Co. Ltd. (Chengdu, China); chitosan was obtained from Sigma-Aldrich (Beijing, China). $HAuCl_4·4H_2O$ was purchased from Alfa Aesar. CEA, anti-CEA and bovine serum albumin (BSA, 96%−99%) were obtained from Dingguo Biochemical Reagents (Beijing, China). PBS (0.1 M) and ultrapure water (18.25 MΩ cm, 24 °C) were used for all of the tests. Chitosan was dissolved in 1% acetic acid. GO/MWCNTs-COOH/Au@CeO_2 were dissolved in 500 μL of 0.5% chitosan.

Apparatus. Scanning electron microscopy (SEM) images and energy-dispersive X-ray spectroscopy (EDS) analysis were collected by using a FEI QUANTA FEG250 coupled with INCA Energy X-MAX-50. X-ray powder diffraction (XRD) was performed with a Bruker D8 Focus diffractometer (Germany). Fourier transform infrared (FTIR) spectra was obtained with a PerkinElmer 580B spectrophotometer (PerkinElmer, United States).The ECL measurements were performed with a MPI-F flow-injection chemiluminescence detector (Xi'an remax Electronic Science Tech. Co. Ltd., China) and electrochemical measurements were carried out on CHI760D electrochemical workstation (Chenhua Instrument Shanghai Co., Ltd., China) by using a three-electrode system.

Preparation of GO. GO was synthesized according to the method reported.[39]

Preparation of GO/MWCNTs-COOH/Au@CeO_2. GO/MWCNTs-COOH@CeO_2 were prepared as described previously with some slight modifications.[22] Five mL of 1 wt % solution of $HAuCl_4·4H_2O$ was added into the mixed solution (GO/MWCNTs-COOH@CeO_2). The suspension was stirred at 90 °C for 6 h and the precipitation was washed by ultrapure water and alcohol. Then the precipitation was dried in vacuum at 40 °C overnight. Lastly, the obtained products (GO/MWCNTs-COOH/Au@CeO_2) were calcined in muffle at 300 °C for 1 h.

Fabrication of the ECL Immunosensor. The construction process was revealed in Scheme 1. First, GCE was handled by alumina powder and washed by ultrapure water. GO/MWCNTs-COOH/Au@CeO_2 were dispersed in 0.5% chitosan after ultrasonication (6 μL, 10.0 mg mL^{-1}). and dropped onto the GCE. GO/MWCNTs-COOH/Au@CeO_2 could be immobilized on the GCE due to the film-forming,[40] stabilizing and nanoparticles protecting properties of chitosan.[41] After drying for 0.5 h, anti-CEA was modified on the film to incubate for 1 h and the electrode was cleaned. The modifed electrode was incubated with BSA (1%, w/w) for 1 h to eliminate nonspecific binding and produce a CEA immunosensor, which was denoted as GO/MWCNTs-COOH/Au@CeO_2/anti-CEA/BSA. After 1 h incubation, the prepared immunosensor was washed. While used for specific determination, GCE was incubated with a series concentrations of CEA solutions (6 μL) for 1 h, washed with ultrapure water, and stored in a 4 °C refrigerator. Therefore, the CEA ECL immunosensor was fabricated successfully.

ECL Response for CEA. The modified electrode was placed in the ECL cell with PBS (10 mL, pH 8, 0.1 M KCl and 120 mM $K_2S_2O_8$). The scanning potential was −2−0 V. PMT was set at 800 V. The scan rate was 0.1 V s^{-1}.

RESULTS AND DISCUSSION

Characterization of GO/MWCNTs-COOH/Au@CeO_2. GO/MWCNTs-COOH/Au@CeO_2 significantly effected the detection of CEA. The structures of GO/MWCNTs-COOH, GO/Au@CeO_2, MWCNTs-COOH/Au@CeO_2 and GO/MWCNTs-COOH/Au@CeO_2 were showed by SEM Figure 1A showed the SEM structure of GO/MWCNTs-COOH. GO and MWCNTs-COOH could provide a large surface-to-volume ratio, which could contain more Au and CeO_2 nanoparticles. The appearance of MWCNTs-COOH could avoid the stacking phenomenon of GO nanosheets.[20] The stability of the sensor was improved due to its better water-solubility than MWCNTs. The efficient electron transfer of MWCNTs-COOH and GO resulted in the ECL signal improvement of CeO_2. As shown in Figure 1B−D, Au@CeO_2 nanoparticles were well-distributed on the surfaces of GO and MWCNTs-COOH, Au nanoparticles were well for combination with anti-CEA via the Au-NH_2 covalent bond.[42] Moreover, Au nanoparticles on the surface of GO/MWCNTs-COOH could also increase the ECL intensity largely, which was important for immunoassay. The

DOI: 10.1021/acsami.5b05185
ACS Appl. Mater. Interfaces 2015, 7, 19260−19267

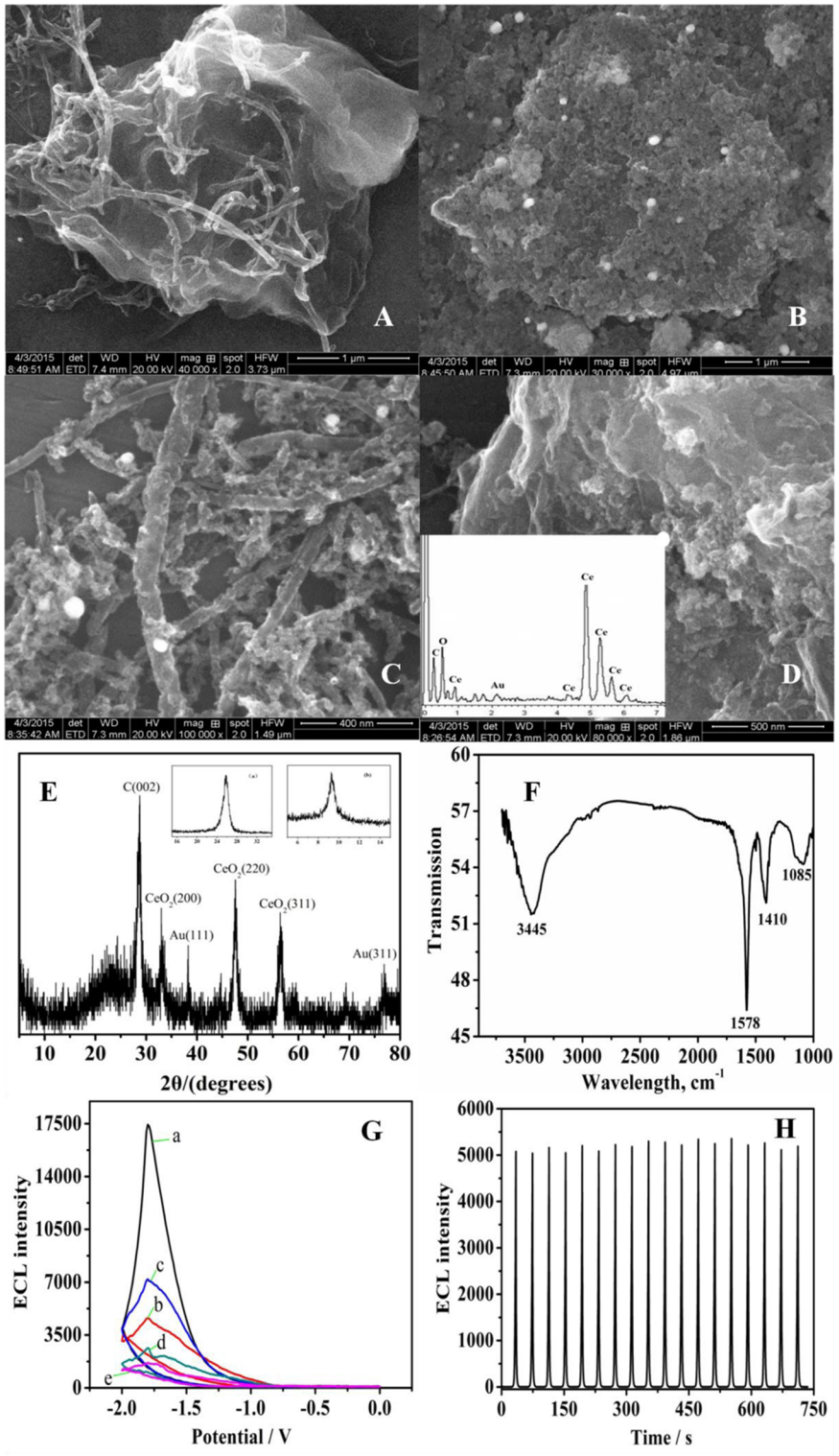

Figure 1. SEM images of (A) GO/MWCNTs-COOH, (B) GO/Au@CeO_2, (C) MWCNTs-COOH/Au@CeO_2, and (D) GO/MWCNTs-COOH/Au@CeO_2 (the inset is EDS of GO/MWCNTs-COOH/Au@CeO_2); (E) XRD patterns of as-synthesized GO/MWCNTs-COOH/Au@CeO_2 (the insets are (a) MWCNTs-COOH and (b) GO); (F) FT-IR spectrometer analysis of GO/MWCNTs-COOH/Au@CeO_2; (G) the ECL intensity-potential curves of different materials: GO/MWCNTs-COOH/Au@CeO_2 (curve a), GO/MWCNTs-COOH/Au (curve b), GO/Au@CeO_2 (curve c), MWCNTs-COOH/Au@CeO_2 (curve d), MWCNTs-COOH/CeO_2 (curve e); (H) the ECL intensity−time curves of CeO_2.

inset was the EDS analysis of GO/MWCNTs-COOH/Au@CeO_2 and C, O, Au, and Ce elements displayed, which demonstrated that the GO/MWCNTs-COOH/Au@CeO_2 were synthesized successfully and the ratio of Au:Ce was ~0.40:15.77.

Figure 1E showed the XRD patterns of as-synthesized GO/MWCNTs-COOH/Au@CeO_2 (the inset are MWCNTs-COOH (a) and GO (b)). The peak at 2θ = 25.94° (002) in inserted Figure 1E (a) was the characteristic peak of MWCNTs-COOH, which was similar to the report.[43] The

DOI: 10.1021/acsami.5b05185
ACS Appl. Mater. Interfaces 2015, 7, 19260−19267

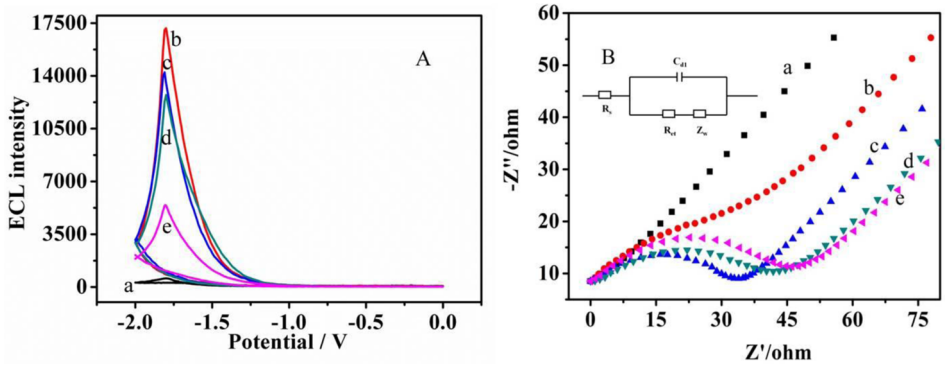

Figure 2. (A) ECL intensity profiles of the bare GCE (curve a), GCE/GO/MWCNTs-COOH/Au@CeO_2 (curve b), GCE/GO/MWCNTs-COOH/Au@CeO_2/anti-CEA (curve c), GCE/GO/MWCNTs-COOH/Au@CeO_2/anti-CEA/BSA (curve d), and GCE/GO/MWCNTs-COOH/Au@CeO_2/anti-CEA/BSA/CEA (curve e) in 0.1 M PBS containing 120 mM $K_2S_2O_8$; (B) EIS of 2.5 mM $[Fe(CN)]_6^{3-/4-}$ at (a) bare GCE, (b) GCE/GO/MWCNTs-COOH/Au@CeO_2, (c) GCE/GO/MWCNTs-COOH/Au@CeO_2/anti-CEA, (d) GCE/GO/MWCNTs-COOH/Au@CeO_2/anti-CEA/BSA, and (e) GCE/GO/MWCNTs-COOH/Au@CeO_2/anti-CEA/BSA/CEA, inset is the equivalent circuit for EIS.

peak at 2θ = 9.26° (002) in inserted Figure 1E (b) was the characteristic peak of GO, which was similar to the report.[44] The peak at 2θ = 28.7° (002) in Figure 1E was the characteristic peak of GO/MWCNTs-COOH, the peak at 2θ = 38.3° (111) was the characteristic peak of Au nanoparticles, the peak at 2θ = 47.58° (220) was the characteristic peak of CeO_2 nanoparticles. In Figure 1E, the aforementioned characteristic peaks also appeared. Besides, the existence of the other peaks indicated the successful combination of GO/MWCNTs-COOH/Au@CeO_2 nanoparticles. GO/MWCNTs-COOH/Au@CeO_2 nanoparticles could be confirmed by FT-IR spectrometer analysis. As shown in Figure 1F, peaks at 1085 and 3445 cm^{-1} was assigned to C−O and O−H stretching vibrations of the carboxylic acid group, respectively,[45] the peaks at 1578 and 1410 cm^{-1} corresponded to C═O and C−O stretching, respectively,[46] which were attributed to the COOH groups onto the external surface of GO/MWCNTs-COOH/Au@CeO_2. Figure 1G displayed the ECL intensity-potential curves of different materials by cycling the potential from −2 to 0 V. Compared with GO/MWCNTs-COOH/Au (curve b), the ECL intensity of GO/MWCNTs-COOH/Au@CeO_2 (curve a) reached a maximum value, which revealed that the strong ECL signals were obtained by CeO_2 with $K_2S_2O_8$. Compared with MWCNTs-COOH/CeO_2 (curve e), MWCNTs-COOH/Au@CeO_2 (curve d) exhibited a better ECL emission, which revealed that Au nanoparticles on the surface of MWCNTs-COOH/CeO_2 could also increase the ECL intensity largely. Compared with MWCNTs-COOH/Au@CeO_2 (curve d) and GO/Au@CeO_2 (curve c), GO/MWCNTs-COOH/Au@CeO_2 exhibited a much stronger ECL emission peak, which might result from the synergistic effect betweeen MWCNTs-COOH and GO.[20] Figure 1H displayed the ECL intensity-time curves of CeO_2. RSD was 1.89% for ECL response, which indicated that CeO_2 could be used well for the luminescence.

ECL Performance. Figure 2A exhibited ECL intensity-potential curves for the electrodes modified by different products. Weak ECL emission for bare GCE can be seen from curve a. However, after GO/MWCNTs-COOH/Au@CeO_2 were modified, better ECL response appeared in curve b. Although the anti-CEA was immobilized on GO/MWCNTs-COOH/Au@CeO_2, ECL response decreased to a certain extent (curve c). ECL response further decreased after modifying BSA (curve d). Laterly, ECL intensity reached a minimum value in curve e when CEA was dropped on GCE. The above phenomenon illustrated that the luminescence property of GO/MWCNTs-COOH/Au@CeO_2 was affected by immunoreaction between antigen and antibody through depressing the diffusion of electrolytes between the solution and the surface of GCE. Accordingly, the label-free ECL immunosensor was fabricated perfectly.

EIS was carried out in 2.5 mM $[Fe(CN)_6]^{3-/4-}$and equivalent circuit as the inset in Figure 2B. The charge transfer resistance (R_{et}), the double layer capacitance (C_{dl}), the Warburg impedance (Z_W) and the resistance of solution (R_s) were given. R_s and Z_W had nothing with the modifications.[47,48] R_{et} changed in the modification processes and can be used as a suitable indicator for displaying the interfacial property. The R_{et} change was related to the resistance of the modified layer on GCE surface, which change reflected by the change of the semicircle diameter (Z') in Nyquist plots. Thus, R_{et} was a selected indicator for explaining the interfacial property of the fabrication process.

EIS curves at different modification steps were shown in Figure 2B. In detail, a small semicircle was observed in curve a due to a free electron-transfer process of the bare GCE. After GO/MWCNTs-COOH/Au@CeO_2 were dropped, curve b showed a smaller. When anti-CEA was subsequently conjugated to the GCE/GO/MWCNTs-COOH/Au@CeO_2 (curve c), semicircle increased obviously because the antibodies suppressed the proton transmission, indicating the antibodies bonded to GO/MWCNTs-COOH/Au@CeO_2 successfully. Curve d exhibited a larger semicircle diameter, clarifying BSA produced the high resistance of the electrode interface. After the successful captured of CEA through specific reaction, a further increment of semicircle domain was observed again (curve e). Thus, the immunosensor was constructed.

ECL mechanism might be as follows:[9,49,50]

CeO_2 accepted e^- to be $CeO_2^{\bullet-}$ (eq 1) when potential changed negatively,. At the same time, $S_2O_8^{2-}$ changed to be $SO_4^{\bullet-}$ and SO_4^{2-} (eq 2) if the potential was negative enough. The excited state of CeO_2* could be generated by the reaction between the strong oxidant $SO_4^{\bullet-}$ and $CeO_2^{\bullet-}$ (eq 3) by the transfer of e^-. When CeO_2* became the ground state (eq 4), the energy was released as light.

$$CeO_2 + \rightarrow CeO_2^{\bullet-} \quad (1)$$

$$S_2O_8^{2-} + e^- \rightarrow SO_4^{2-} + SO_4^{\bullet-} \quad (2)$$

DOI: 10.1021/acsami.5b05185
ACS Appl. Mater. Interfaces 2015, 7, 19260−19267

$$CeO_2^{\bullet -} + SO_4^{\bullet -} \rightarrow CeO_2^* + SO_4^{2-} \quad (3)$$

$$CeO_2^* \rightarrow CeO_2 + h\nu \quad (4)$$

Optimization of Experimental Conditions. We investigated the concentration of GO/MWCNTs-COOH/Au@CeO_2 and $K_2S_2O_8$, pH value, and scan rates. ECL intensity enhanced from 2.0 to 10.0 mg mL^{-1} and showed the maximum value at 10.0 mg mL^{-1} (Figure 3A). Then, with a further increase in the concentration from 10.0 to 14.0 mg mL^{-1} of GO/MWCNTs-COOH/Au@CeO_2, ECL intensity turned down. The excessive GO/MWCNTs-COOH/Au@CeO_2 may be stacked each other resulting in the electron transfer hindered. Therefore, 10 mg mL^{-1} was selected for subsequent experiments. pH was invesitigated from 5.0 to 8.5 (Figure 3B) and ECL showed the best performance at pH 8.0. Almost neutral environment benefited the ECL performance. So 8.0 was selected. The effect of coreactant $K_2S_2O_8$ concentrations from 20 mM to 140 mM was investigated (Figure 3C). When the concentration of $K_2S_2O_8$ was 120 mM, ECL response showed the maximum response.The ECL intensity (Figure 3D) showed the same change pattern with other ECL sensor[51] at a scan rate of 0.10−0.20 V s^{-1} with a increment of 0.04−0.10 V s^{-1}. The diffusion rate of and the formation rate of CeO_2* dominated ECL efficiency.[52] At high scan rates on the electrode interface, the consumption of $K_2S_2O_8$ was much quicker than its diffusion. Then less $K_2S_2O_8$ resulted in the reducement of ECL response. In a word, low ECL response was related with the high scan rate. Therefore, 0.10 V s^{-1} was optimized.

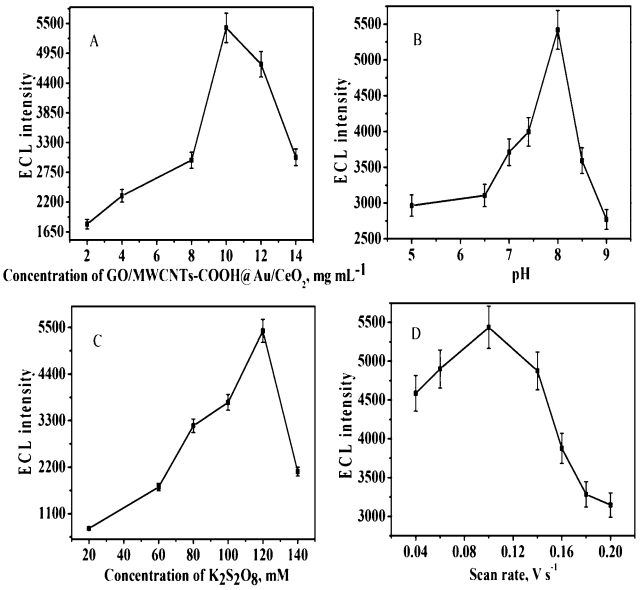

Figure 3. Effect of (A) GO/MWCNTs-COOH/Au@CeO_2, (B) pH, (C) $K_2S_2O_8$, and (D) scan rates on the response of ECL intensity from GCE/GO/MWCNTs-COOH/Au@CeO_2/anti-CEA/BSA/CEA (error bar = SD, n = 3).

Performance of the Immunosensor. GO/MWCNTs-COOH/Au@CeO_2 was used as the substrate for the determination of CEA (Figure 4A). ECL immunosensor is constructed on the antigen−antibody specific recognition. The electron transfer could be hindered by the proteins and the ECL response decreased with the increase of concentrations of CEA. As Figure 4B showed, ECL intensity reduced with the linearly increase of logarithm of CEA concentration from 0.05−100 ng/mL. The equation of the calibration curve was I = 7261.045−2881.511 log[c] (R = 0.994). The lower LOD (0.02 ng/mL, signal-to-noise ratio = 3) might be related with the ECL signal amplification of GO/MWCNTs-COOH and Au nanoparticles. A comparison with other sensors for CEA was given in Table 1.[32,53−57] The LOD and linear range were

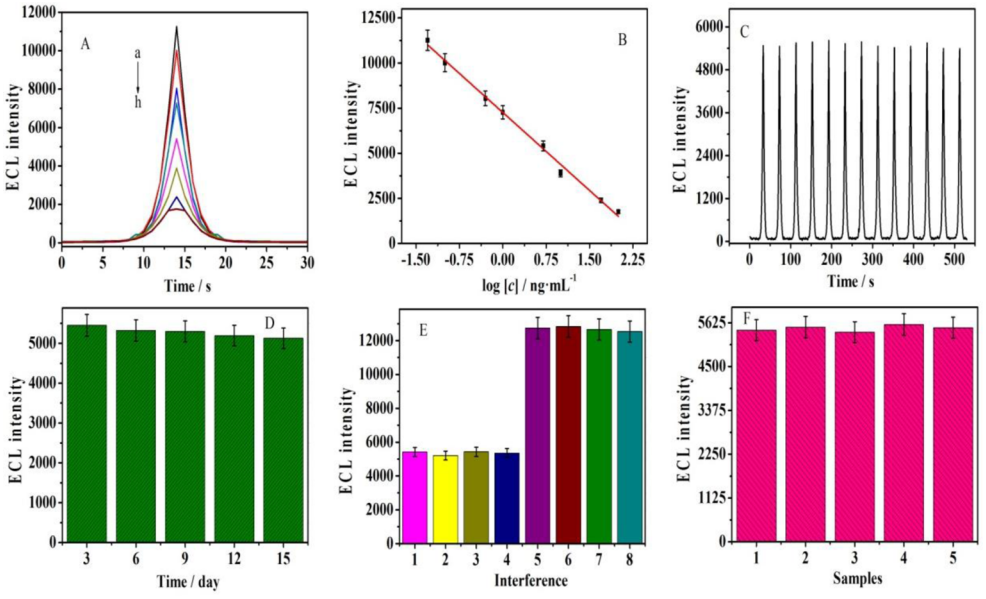

Figure 4. (A) ECL response of the ECL sensor to different concentrations of CEA, from a to g: 0.05, 0.1, 0.5, 1.0, 5.0, 10.0, 50.0, 100 ng/mL. (B) Calibration curve of the ECL sensor for CEA at different concentrations. (C) ECL intensity of the GCE/GO/MWCNTs-COOH/Au@CeO_2/anti-CEA/BSA/CEA in PBS (pH 8.0) containing 0.1 M KCl under continuous scanning for 13 cycles. (D) Long-term storage stability of GCE/GO/MWCNTs-COOH/Au@CeO_2/anti-CEA/BSA/CEA as a function of different time interval in PBS (pH 8.0) containing 0.1 M KCl and 5 ng/mL CEA. (E) ECL intensity of the ECL sensor to 5 ng/mL CEA (1), 5 ng/mL CEA + 500 ng/mL PSA (2), 5 ng/mL CEA + 500 ng/mL BSA (3), 5 ng/mL CEA + 500 ng/mL AFP (4), 0 ng/mL CEA (5), 5 ng/mL PSA (6), 5 ng/mL BSA (7), 5 ng/mL AFP (8). (Error bar = SD, n = 3). (F) Repeatability of the GCE/GO/MWCNTs-COOH/Au@CeO_2/anti-CEA/BSA/CEA in PBS (pH 8.0) containing 0.1 M KCl and 5 ng/mL CEA.

DOI: 10.1021/acsami.5b05185
ACS Appl. Mater. Interfaces 2015, 7, 19260−19267

Table 1. Comparison of the Performance of the Proposed and Referenced Sensors for CEA

material of sensors	method	linear range (ng mL^{-1})	detection limit (ng mL^{-1})	refs
immunogold−silver	ICPMS	0.1−40.0	0.1	53
Au-TiO_2 particle	CV	1.0−100	0.53	54
AuNPs-PAMAM/PEI-rGO	CL	1.0−70	0.65	55
AuPt nanochains	CV	0.01−200	0.0011	56
Fe_3O_4 nanoparticles	ECL	1.0−780	0.28	57
CdTe/CdS quantum dots	fluorescent	0.045−45000	0.0045	32
this work	ECL	0.05−100	0.02	-

compared. Although the immunosensor developed by Cao[56] had lower LOD than the one in this work, the proposed immunosensor was faster and easier to use. In addition, Wang & Fan[36,58,59] have reported a very sensitive method for CEA detection. Meanwhile, the immunosensor widened the use range of CeO_2 and provided a novel way for CEA detection.

Stability, Selectivity, and Repeatability of ECL Response. Stability was an important parameter in practical use of all of the chemical sensors. ECL response of the GO/MWCNTs-COOH/Au@CeO_2 was displayed (Figure 4C) under 13 cycles from −2 to 0 at 0.1 V s^{-1} in PBS (pH 8.0, 0.1 M KCl, 120 mM $K_2S_2O_8$). RSD of 1.85% indicated good detection performance and good operational stability. In addition, the long-term storage stability was investigated at 5 ng/mL CEA stored at 4 °C and tested every 3 days. As Figure 4D showed, outstanding long-term stability was concluded from the following tests: ECL intensity kept constant after storing in the PBS in a 4 °C refrigerator for 3 days, ECL intensity reduced almost 2.8% after storage for 9 days and 5.9% after 15 days. To inspect the selectivity of the label-free ECL immunosensor, the interferences of prostate specific antigen (PSA), bovine serum albumin (BSA) and alpha-fetoprotein (AFP) were investigated for the determination of CEA. It could be found that PSA, BSA and AFP (500 ng/mL) did not interfere the detection of CEA at 5 ng/mL. The results (Figure 4E) indicated the accredited selectivity of the label-free ECL immunosensor.

The repeatability of the label-free ECL immunosensor was also inspected. RSD of measurements was 1.37% by five electrodes with 5 ng/mL CEA (Figure 4F), suggesting that the label-free ECL immunosensor had satisfied repeatability.

Application Analysis in Human Serum Samples. The practical application feasibility was studied by detecting human serum samples. The serum samples were appropriately diluted by PBS (pH 8.0), because the tumor marker level of serum was higher than the calibration range. As shown in Table 2, different concentrations (5.00, 10.00, 20.00, 6.00, 15.00 ng/mL) of standard CEA solutions were put into human serum samples according to standard addition method. The RSD was 1.85−4.40% and recoveries were 98.9−102.6%. The results suggested the immunosensor could be used to detect CEA in serum samples.

CONCLUSION

A label-free ECL immunosensor was fabricated by using GO/MWCNTs-COOH/Au@CeO_2, which was first used in ECL sensor assay. CeO_2 nanoparticles were used with $K_2S_2O_8$ in ECL field for the first time. GO/MWCNTs-COOH/Au nanoparticles accelerated the electrons transfer and improved ECL response largely. The proposed label-free ECL immunosensor exhibited acceptable selectivity, long-term stability, and wide linear range. And what's more, the label-free immunosensor will promote the further use of CeO_2 nanoparticles in the biosensing field.

Table 2. Recovery of the Proposed Label-Free ECL Immunosensor in Human Serum Samples

serum samples (ng mL^{-1})	addition content (ng mL^{-1})	detection content (ng mL^{-1})	avg value (ng mL^{-1})	RSD (%)	recovery (%)
2.24	5.00	7.17, 7.53, 7.42, 7.29, 7.38	7.358	1.85	101.6
	10.00	11.92, 12.31, 12.48, 12.14, 13.09	12.388	3.58	101.2
	20.00	20.85, 21.34, 23.27, 22.61, 21.92	21.998	4.40	98.9
6.12	6.00	11.75, 12.46, 12.28, 11.81, 12.16	12.092	2.52	99.8
	15.00	20.91, 22.65, 21.75, 22.18, 20.87	21.672	3.61	102.6

AUTHOR INFORMATION

Corresponding Authors

*E-mail: sdjndxwq@163.com. Tel.: +86 531 82767872. Fax: +86 531 82765969.

*E-mail: mahongmin2002@126.com.

Notes

The authors declare no competing financial interest.

ACKNOWLEDGMENTS

This study was supported by the Natural Science Foundation of China (21175057, 21375047, 21377046, 21575050, 21505051), the Science and Technology Plan Project of Jinan (201307010), and the Science and Technology Development Plan of Shandong Province (2014GSF120004). Q.W. thanks the Special Foundation for Taishan Scholar Professorship of Shandong Province and UJN (ts20130937).

REFERENCES

(1) Ji, J.; He, L.; Shen, Y.; Hu, P.; Li, X.; Jiang, L. P.; Zhang, J. R.; Li, L. L.; Zhu, J. J. High-efficient Energy Funneling Based on Electrochemiluminescence Resonance Energy Transfer in Graded-gap Quantum Dots Bilayers for Immunoassay. *Anal. Chem.* **2014**, *86*, 3284−3290.

(2) Jie, G.; Wang, L.; Yuan, J.; Zhang, S. Versatile Electrochemiluminescence Assays for Cancer Cells Based on Dendrimer/CdSe-ZnS-quantum Dot Nanoclusters. *Anal. Chem.* **2011**, *83*, 3873−3880.

(3) Ding, C. C.; Zheng, Q.; Wang, N.; Yue, Q. An Electrochemiluminescence Strategy Based on Aptamers and Nanoparticles for the Detection of Cancer Cells. *Anal. Chim. Acta* **2012**, *756*, 73−78.

(4) Ding, C. C.; Wei, S.; Liu, H. Electrochemiluminescent Determination of Cancer Cells Based on Aptamers, Nanoparticles, and Magnetic Beads. *Chem. - Eur. J.* **2012**, *18*, 7263−7268.

(5) Kim, Y.; Kim, J. Modification of Indium Tin Oxide with Dendrimer-encapsulated Nanoparticles to Provide Enhanced Stable Electrochemiluminescence of $Ru(bpy)_3^{2+}$/tripropylamine While Preserving Optical Transparency of Indium Tin Oxide for Sensitive Electrochemiluminescence-based Analyses. *Anal. Chem.* **2014**, *86*, 1654−1660.

DOI: 10.1021/acsami.5b05185
ACS Appl. Mater. Interfaces 2015, 7, 19260−19267

(6) Li, F.; Cui, H. A Label-free Electrochemiluminescence Aptasensor for Thrombin Based on Novel Assembly Strategy of Oligonucleotide and Luminol Functionalized Gold Nanoparticles. *Biosens. Bioelectron.* **2013**, *39*, 261−267.
(7) Jie, G. F.; Liu, B.; Miao, J. J.; Zhu, J. J. Electrogenerated Chemiluminescence from CdS Nanotubes and Its Sensing Application in Aqueous Solution. *Talanta* **2007**, *71*, 1476−1480.
(8) Ren, T.; Xu, J. Z.; Tu, Y. F.; Xu, S.; Zhu, J. J. Electrogenerated Chemiluminescence of CdS Spherical Assemblies. *Electrochem. Commun.* **2005**, *7*, 5−9.
(9) Jie, G.; Zhang, J.; Wang, D.; Cheng, C.; Chen, H. Y.; Zhu, J. J. Electrochemiluminescence Immunosensor Based on CdSe Nanocomposites. *Anal. Chem.* **2008**, *80*, 4033−4039.
(10) Liu, B.; Ren, T.; Zhang, J. R.; Chen, H. Y.; Zhu, J. J.; Burda, C. Spectroelectrochemistry of Hollow Spherical CdSe Quantum Dot Assemblies in Water. *Electrochem. Commun.* **2007**, *9*, 551−557.
(11) Liu, X.; Jiang, H.; Lei, J.; Ju, H. X. Anodic Electrochemiluminescence of CdTe Quantum Dots and Its Energy Transfer for Detection of Catechol Derivatives. *Anal. Chem.* **2007**, *79*, 8055−8060.
(12) Ding, C. C.; Zhong, H.; Zhang, S. S. Ultrasensitive Flow Injection Chemiluminescence Detection of DNA Hybridization Using NanoCuS Tags. *Biosens. Bioelectron.* **2008**, *23*, 1314−1318.
(13) Geng, J.; Jia, X. D.; Zhu, J. J. Sonochemical Selective Synthesis of ZnO/CdS Core/shell Nanostructures and Their Optical Properties. *CrystEngComm* **2011**, *13*, 193−198.
(14) Kaushik, A.; Solanki, P. R.; Pandey, M.; Ahmad, S.; Malhotra, B. D. Cerium Oxide-chitosan Based Nanobiocomposite for Food Borne Mycotoxin Detection. *Appl. Phys. Lett.* **2009**, *95*, 173703−3.
(15) Estévez-Hernández, O.; Cisneros, J. H.; Reguera, E.; Naranjo-Rodríguez, I. On the Complex Formation of $CdCl_2$ with 1-furoylthioureas: Preconcentration and Voltammetric Behavior of Cd (II) at Carbon Paste Electrodes Modified with 3-monosubstituted and 3, 3-disubstituted Derivatives. *Sens. Actuators, B* **2007**, *120*, 766−772.
(16) Kaushik, A.; Solanki, P. R.; Ansari, A. A.; Ahmad, S.; Malhotra, B. D. Chitosan-iron Oxide Nanobiocomposite Based Immunosensor for Ochratoxin-A. *Electrochem. Commun.* **2008**, *10*, 1364−1368.
(17) Chu, Y. Y.; Wang, Z. B.; Jiang, Z. Z.; Gu, D. M.; Yin, G. P. A Novel Structural Design of a Pt/C-CeO_2 Catalyst with Improved Performance for Methanol Electro-oxidation by β-cyclodextrin Carbonization. *Adv. Mater.* **2011**, *23*, 3100−3104.
(18) Qiu, J. D.; Cui, S. G.; Liang, R. P. Hydrogen Peroxide Biosensor Based on the Direct Electrochemistry of Myoglobin Immobilized on Ceria Nanoparticles Coated with Multiwalled Carbon Nanotubesby a Hydrothermal Synthetic Method. *Microchim. Acta* **2010**, *171*, 333−339.
(19) Saha, S.; Arya, S. K.; Singh, S.; Sreenivas, K.; Malhotra, B.; Gupta, V. Nanoporous Cerium Oxide Thin Film for Glucose Biosensor. *Biosens. Bioelectron.* **2009**, *24*, 2040−2045.
(20) Peng, L.; Feng, Y.; Lv, P.; Lei, D.; Shen, Y.; Li, Y.; Feng, W. Transparent, Conductive, and Flexible Multiwalled Carbon Nanotube/graphene Hybrid Electrodes with Two Three-dimensional Microstructures. *J. Phys. Chem. C* **2012**, *116*, 4970−4978.
(21) Cheng, Q.; Tang, J.; Ma, J.; Zhang, H.; Shinya, N.; Qin, L. C. Graphene and Carbon Nanotube Composite Electrodes for Supercapacitors with Ultra-high Energy Density. *Phys. Chem. Chem. Phys.* **2011**, *13*, 17615−17624.
(22) Rajendran, R.; Shrestha, L. K.; Minami, K.; Subramanian, M.; Jayavel, R.; Ariga, K. Dimensionally Integrated Nanoarchitectonics for a Novel Composite from 0D, 1D, and 2D Nanomaterials: RGO/CNT/CeO_2 Ternary Nanocomposites with Electrochemical Performance. *J. Mater. Chem. A* **2014**, *2*, 18480−18487.
(23) Rakhi, R.; Alshareef, H. Enhancement of the Energy Storage Properties of Supercapacitors Using Graphene Nanosheets Dispersed with Metal Oxide-loaded Carbon Nanotubes. *J. Power Sources* **2011**, *196*, 8858−8865.
(24) Zhang, B.; Zheng, Q. B.; Huang, Z. D.; Oh, S. W.; Kim, J. K. SnO_2-graphene-carbon Nanotube Mixture for Anode Material with Improved Rate Capacities. *Carbon* **2011**, *49*, 4524−4534.
(25) Xiao, Y.; Zhang, Q.; Yan, J.; Wei, T.; Fan, Z.; Wei, F. Compressible Aligned Carbon Nanotube/MnO_2 as High-rate Electrode Materials for Supercapacitors. *J. Electroanal. Chem.* **2012**, *684*, 32−37.
(26) Lota, G.; Fic, K.; Frackowiak, E. Carbon Nanotubes and Their Composites in Electrochemical Applications. *Energy Environ. Sci.* **2011**, *4*, 1592−1605.
(27) Kim, Y. T.; Tadai, K.; Mitani, T. Highly Dispersed Ruthenium Oxide Nanoparticles on Carboxylated Carbon Nanotubes for Supercapacitor Electrode Materials. *J. Mater. Chem.* **2005**, *15*, 4914−4921.
(28) Jie, G.; Liu, P.; Wang, L.; Zhang, S. S. Electrochemiluminescence Immunosensor Based on Nanocomposite Film of CdS Quantum Dots-carbon Nanotubes Combined with Gold Nanoparticles-chitosan. *Electrochem. Commun.* **2010**, *12*, 22−26.
(29) Tang, D.; Yuan, R.; Chai, Y. Ultrasensitive Electrochemical Immunosensor for Clinical Immunoassay Using Thionine-doped Magnetic Gold Nanospheres as Labels and Horseradish Peroxidase as Enhancer. *Anal. Chem.* **2008**, *80*, 1582−1588.
(30) Rusling, J. F.; Sotzing, G.; Papadimitrakopoulosa, F. Designing Nanomaterial-enhanced Electrochemical Immunosensors for Cancer Biomarker Proteins. *Bioelectrochemistry* **2009**, *76*, 189−194.
(31) Li, C.; Lin, J.; Guo, Y.; Zhang, S. S. A Novel Electrochemiluminescent Reagent of Cyclometalated Iridium Complex-based DNA Biosensor and Its Application in Cancer Cell Detection. *Chem. Commun.* **2011**, *47*, 4442−4444.
(32) Hu, M.; Yan, J.; He, Y.; Lu, H. T.; Weng, L. X.; Song, S. P.; Fan, C. H.; Wang, L. H. Ultrasensitive, Multiplexed Detection of Cancer Biomarkers Directly in Serum by Using a Quantum Dot-Based Microfluidic Protein Chip. *ACS Nano* **2009**, *4*, 488−494.
(33) Huang, K. H. G.; Bonsall, D.; Katzourakis, A.; Thomson, E. C.; Fidler, S. J.; Main, J.; Muir, D.; Weber, J. N.; Frater, A. J.; Phillips, R. E.; Pybus, O. G.; Goulder, J. R.; Mclure, M. O.; Cooke, G. S.; Klenerman, P. B-cell Depletion Reveals a Role for Antibodies in the Control of Chronic HIV-1 Infection. *Nat. Commun.* **2010**, *1*, 102.
(34) Naghibalhossaini, F.; Ebadi, P. Evidence for CEA Release from Human Colon Cancer Cells by an Endogenous GPI-PLD Enzyme. *Cancer Lett.* **2006**, *234*, 158−167.
(35) Li, R.; Feng, F.; Chen, Z. Z.; Bai, Y. F.; Guo, F. F.; Wu, F. Y.; Zhou, G. Sensitive Detection of Carcinoembryonic Antigen Using Surface Plasmon Resonance Biosensor with Gold Nanoparticles Signal Amplification. *Talanta* **2015**, *140*, 143−149.
(36) Giljohann, D. A.; Seferos, D. S.; Patel, P. C.; Millstone, J. E.; Rosi, N. L.; Mirkin, C. A. Oligonucleotide Loading Determines Cellular Uptake of DNA-modified Gold Nanoparticles. *Nano Lett.* **2007**, *7*, 3818−3821.
(37) Souza, G. R.; Christianson, D. R.; Staquicini, F. I.; Ozawa, M. G.; Snyder, E. Y.; Sidman, R. L. Networks of Gold Nanoparticles and Bacteriophage as Biological Sensors and Cell-targeting Agents. *Proc. Natl. Acad. Sci. U. S. A.* **2006**, *103*, 1215−1220.
(38) Murphy, C. J.; Gole, A. M.; Stone, J. W.; Sisco, P. N.; Alkilany, A. M.; Goldsmith, E. C. Gold Nanoparticles in Biology: Beyond Toxicity to Cellular Imaging. *Acc. Chem. Res.* **2008**, *41*, 1721−1730.
(39) Marcano, D. C.; Kosynkin, D. V.; Berlin, J. M.; Sinitskii, A.; Sun, Z.; Slesarev, A.; Alemany, L. B.; Lu, W.; Tour, J. M. Improved Synthesis of Graphene Oxide. *ACS Nano* **2010**, *4*, 4806−4814.
(40) Muzzarelli, R. A.; Tanfani, F.; Scarpini, G. Chelating, Film - forming, and Coagulating Ability of the Chitosan-glucan Complex from Aspergillus Niger Industrial Wastes. *Biotechnol. Bioeng.* **1980**, *22*, 885−896.
(41) Huang, H.; Yang, X. Chitosan Mediated Assembly of Gold Nanoparticles Multilayer. *Colloids Surf., A* **2003**, *226*, 77−86.
(42) Kristensen, I. S.; Mowbray, D.; Thygesen, K. S.; Jacobsen, K. W. Comparative Study of Anchoring Groups for Molecular Electronics: Structure and Conductance of Au-S-Au and Au-NH_2-Au Junctions. *J. Phys.: Condens. Matter* **2008**, *20*, 374101.
(43) Song, H. Q.; Zhu, Q.; Zheng, X. J.; Chen, X. G. One-step Synthesis of Three-dimensional Graphene/multiwalled Carbon Nano-

DOI: 10.1021/acsami.5b05185
ACS Appl. Mater. Interfaces 2015, 7, 19260−19267

tubes/Pd Composite Hydrogels: an Efficient Recyclable Catalyst for Suzuki Coupling Reactions. *J. Mater. Chem. A* **2015**, *3*, 10368−10377.
(44) Chen, S.; Yeoh, W.; Liu, Q.; Wang, G. Chemical-free Synthesis of Graphene-carbon Anotube Hybrid Materials for Reversible Lithium Storage in Lithium-ion Batteries. *Carbon* **2012**, *50*, 4557−4565.
(45) Zhang, J.; Zou, H.; Qing, Q.; Yang, Y.; Li, Q.; Liu, Z.; Guo, X. Y.; Du, Z. L. Effect of Chemical Oxidation on the Structure of Single-walled Carbon Nanotubes. *J. Phys. Chem. B* **2003**, *107*, 3712−3718.
(46) Arvand, M.; Hassannezhad, M. Magnetic Core-shell Fe_3O_4@ SiO_2/MWCNT Nanocomposite Modified Carbon Paste Electrode for Amplified Electrochemical Sensing of Uric Acid. *Mater. Sci. Eng., C* **2014**, *36*, 160−167.
(47) Huang, H.; Ran, P.; Liu, Z. Impedance Sensing of Allergen-antibody Interaction on Glassy Carbon Electrode Modified by Gold Electrodeposition. *Bioelectrochemistry* **2007**, *70*, 257−262.
(48) Yang, L.; Li, Y. AFM and Impedance Spectroscopy Characterization of the Immobilization of Antibodies on Indium-tin Oxide Electrode Through Self-assembled Monolayer of Epoxysilane and Their Capture of Escherichia Coli O157: H7. *Biosens. Bioelectron.* **2005**, *20*, 1407−1416.
(49) Lu, Q.; Wei, W.; Zhou, Z. X.; Zhou, Z. X.; Zhang, Y. J.; Liu, S. Q. Electrochemiluminescence Resonance Energy Transfer Between Graphene Quantum Dots and Gold Nanoparticles for DNA Damage Detection. *Analyst* **2014**, *139*, 2404−2410.
(50) Qian, J.; Zhang, C. Y.; Cao, X. D.; Liu, S. Q. Versatile Immunosensor Using a Quantum Dot Coated Silica Nanosphere as a Label for Signal Amplification. *Anal. Chem.* **2010**, *82*, 6422−6429.
(51) Zou, G.; Ju, H. X. Electrogenerated Chemiluminescence from a CdSe Nanocrystal Film and Its Sensing Application in Aqueous Solution. *Anal. Chem.* **2004**, *76*, 6871−6876.
(52) Cheng, C. M.; Huang, Y.; Tian, X. Q.; Zheng, B. Z.; Li, Y.; Yuan, H. Y.; Xiao, D.; Xie, S. P.; Choi, M. F. Electrogenerated Chemiluminescence Behavior of Graphite-like Carbon Nitride and Its Application in Selective Sensing Cu^{2+}. *Anal. Chem.* **2012**, *84*, 4754−4759.
(53) Liu, R.; Liu, X.; Tang, Y.; Wu, L.; Hou, X.; Lv, Y. Highly Sensitive Immunoassay Based on Immunogold-silver Amplification and Inductively Coupled Plasma Mass Spectrometric Detection. *Anal. Chem.* **2011**, *83*, 2330−2336.
(54) Zhang, Y.; Yuan, R.; Chai, Y.; Xiang, Y.; Qian, X.; Zhang, H. Sensitive Label-free Immunoassay of Carcinoembryonic Antigen Based on Au-TiO_2 Hybrid Nanocomposite Film. *J. Colloid Interface Sci.* **2010**, *348*, 108−113.
(55) Dungchai, W.; Siangproh, W.; Lin, J. M.; Chailapakul, O.; Lin, S.; Ying, X. Development of a Sensitive Micro-magnetic Chemiluminescence Enzyme Immunoassay for the Determination of Carcinoembryonic Antigen. *Anal. Bioanal. Chem.* **2007**, *387*, 1965−1971.
(56) Cao, X.; Wang, N.; Jia, S.; Guo, L.; Li, K. Bimetallic AuPt Nanochains: Synthesis and Their Application in Eelectrochemical Immunosensor for the Detection of Carcinoembryonic Antigen. *Biosens. Bioelectron.* **2013**, *39*, 226−230.
(57) Huang, G.; Deng, B.; Xi, Q.; Tao, C.; Ye, L. Surface Modification of Superparamagnetic Magnetite Nanoparticles and Its Application for Detection of Anti-CEA Using Electrochemiluminescent Immunosensor. *Med. Chem.* **2015**, *5*, 050−057.
(58) Yan, J.; Song, S.; Li, B.; Zhang, Q. Z.; Huang, Q.; Zhang, H.; Fan, C. H. An On-nanoparticle Rolling-circle Amplification Platform for Ultrasensitive Protein Detection in Biological Fluids. *Small* **2010**, *6*, 2520−2525.
(59) Hu, M.; He, Y.; Song, S.; Yan, J.; Lu, H. T.; Weng, L. X.; Wang, L. H.; Fan, C. H. DNA-bridged Bioconjugation of Fluorescent Quantum Dots for Highly Sensitive Microfluidic Protein Chips. *Chem. Commun.* **2010**, *46*, 6126−6128.

DOI: 10.1021/acsami.5b05185
ACS Appl. Mater. Interfaces 2015, 7, 19260−19267